

Analysis of Charge Asymmetry in Rare Dilepton B Decays

Dongsheng Liu

Department of Physics, University of Tasmania

Hobart, AUSTRALIA 7001

(1 March, 1995)

Abstract

We analyze forward-backward charge asymmetry of the lepton production in rare decays $B \rightarrow X_s l^+ l^-$ and $B \rightarrow K^* l^+ l^-$, including vector-resonance effects. Certain regions of phase space, in which the asymmetry is sensitive to individual short-distance coefficients, are pointed out. In particular, we suggest a method to test the coupling of the leptonic axial vector current to the left-handed quark current experimentally.

11.30-j, 11.30.Cp, 11.30.Ly, 12.50.Ch

arXiv:hep-ph/9505314v2 16 May 1995

I. INTRODUCTION

Rare B decays have been the focus of many experimental and theoretical considerations [1,2]. This is due to the amount of information on the standard model that can be extracted from these processes. The rare decays proceed through flavor-changing neutral current diagrams that are absent at the tree level and thus provide a good probe of the standard model at the loop level. For example, recent measurements of photon penguin induced processes $B \rightarrow X_s \gamma$ and $B \rightarrow K^* \gamma$ by the CLEO group [1] are consistent with the standard model predictions. Likewise, the dilepton decay $B \rightarrow X_s l^+ l^-$ and corresponding exclusive modes will provide tests of the Z boson penguin and W boson box diagrams which take over the photonic penguin diagram for large top quark mass. On the other hand, unlike the radiative B decays, the dileptonic processes are strongly dependent on the top quark mass m_t through the dominant internal top quark line, so that a comparison between theoretical calculations as a function of m_t and experimental data may lead to constraints on the top quark mass. Such an exercise has been done with the current upper limit of $\text{Br}(b \rightarrow s \mu^+ \mu^-) < 5.0 \times 10^{-5}$ (90% CL), which gives the bound of ~ 390 GeV on the top quark mass [3]. These rare B decays are also sensitive to quark mixing angles V_{td} , V_{ts} and V_{tb} , hence their measurements yield valuable information on Cabibbo-Kobayashi-Maskawa (CKM) matrix elements and consequently shed some light on CP violation in the standard model. In this work we concentrate on the rare dileptonic decay $b \rightarrow s l^+ l^-$ (l is either an electron or a muon.).

While extensive investigations have been carried out for the invariant mass spectrum of dileptons, the authors of Ref. [4] pointed out that to fully extract short-distance coefficients both in magnitude and in sign from experiments, one has to consider the angular distribution such as forward-backward charge asymmetry of the l^+ production in the decay $b \rightarrow s l^+ l^-$, either. In addition, this asymmetry can be used to test the chirality of the $b \rightarrow s$ transition. The process $B \rightarrow K^* l^+ l^-$ has been considered for the small recoil case where heavy quark symmetries apply [5,6]. Recently, the Dalize distribution of the exclusive rare

dilepton decays has been derived in terms of various form factors [7] and the sensitivity of it to possible new physics has been investigated. In particular, it is shown that measurement of the transverse polarization of K^* meson yields information on the coupling of the leptonic axial vector current to the left-handed quark current. It is the aim of this work to provide a comprehensive analysis of asymmetry for both inclusive process $B \rightarrow X_s l^+ l^-$ and exclusive channel $B \rightarrow K^* l^+ l^-$ in the context of the standard model. We attempt to probe kinematic regions in which asymmetries are sensitive to individual short-distance coefficients. Thus measurements of these asymmetries provide tests of short-distance physics which is sensitive to extensions of the standard model. In this context it is suitable to consider the *integral* asymmetry as we have flexibility to make various phase space cuts and read off the corresponding ‘partial integrated’ asymmetry.

The forward-backward asymmetry results from the interference of leptons produced by the vector current with that by the axial vector current (see Eq. (10)). This is because it is a parity violating effect. In the $b \rightarrow s l^+ l^-$, the axial vector current is mainly due to the Z boson penguin and W boson box diagrams in which top quarks are involved. The vector current arises not only from these two diagrams along with the photon penguin one, but also from loops containing instead charm quarks. Extensions of the standard model lead to extra diagrams. In models with two Higgs doubles, for example, there is a charged scalar particle. The charged scalar coupling to quarks can substitute W boson in the Z boson penguin diagram. In addition to these, resonances such as the J/ψ and ψ' , created by the neutral four-quark operator $b s c \bar{c}$, contribute to the vector current via the $V \rightarrow l^+ l^-$. As shown later on, different sources of the vector current manifest themselves in different regions of phase space, whereas the axial vector current is constant overall. For the very low q^2 the photonic penguin dominates, while the Z penguin and W box becomes important towards high q^2 . Furthermore, we shall demonstrate in this work that the short-distance component of the vector current suffers from cancellation dramatically in the middle q^2 region. Actually, the pure top quarks effect vanishes at an invariant mass close to the J/ψ mass and the analogy can be made with nonresonant contributions near

the ψ' . Thus the asymmetry over there, roughly speaking, contains two factors; one is from top quarks responsible for the axial vector current, and another is from charm quarks for the vector current. The former is short-distance and sensitive to new physics, while the latter, we believe, remains unchanged in extensions of the standard model. As it is not renormalized under QCD, the effective axial vector vertex can be calculated reliably. On the other hand, calculations show that the Wilson coefficient of the $b\bar{s}c\bar{c}$ operator, denoted by a_2 , is sensitive to the QCD scale parameter and the renormalization point and scheme beyond the leading logarithmic approximation [8]. But it is hopeful phenomenologically to extract this coefficient quite precisely from nonleptonic B decays. With the top mass from the Fermilab and the value of a_2 determined by the data of the $B \rightarrow X_s J/\psi$, the standard model prediction for forward-backward asymmetry of the middle region is insensitive to the dependence on the QCD renormalization parameters. Meanwhile, measurements of the asymmetry offer us an opportunity to detect the axial current in the $b \rightarrow sl^+l^-$ and to set constraints on extensions of the standard model. We suggest therefore that one should home in on the resonant region for revealing the effect of the axial vector current and short-distance physics in general. This is contrast to the decay rate spectrum where one has to ‘cut out’ J/ψ and ψ' resonances to probe the short-distance effect.

This paper is organized as follows. We will briefly review the effective Hamiltonian for the flavor-changing neutral-current-induced transition $b \rightarrow sl^+l^-$ in the following section. Then we proceed into the analysis of forward-backward asymmetry of the inclusive process $B \rightarrow X_s l^+l^-$ in Sec. III. The exclusive channel $B \rightarrow K^* l^+l^-$ is also examined in the section, by employing heavy quark symmetry to determine form factors from measurements of semileptonic D decays. Sec. IV is devoted to relevant discussions along with our conclusion. An Appendix contains some useful integral formulae occurred in the main text.

II. EFFECTIVE HAMILTONIAN

Let us begin with an effective Hamiltonian relevant to flavor-changing one-loop processes $b \rightarrow sl^+l^-$ [9],

$$H_{\text{eff}} = \frac{G_F}{\sqrt{2}} \left(\frac{\alpha}{4\pi s_W^2} \right) [\bar{s}\Gamma_\mu^A b \bar{l}\gamma^\mu(1 - \gamma_5)l + \bar{s}\Gamma_\mu^B b \bar{l}\gamma^\mu(1 + \gamma_5)l], \quad (1)$$

with effective vertices,

$$\Gamma_\mu^{A(B)} = A(B)\gamma_\mu(1 - \gamma_5) - im_b s_W^2 F_2 \sigma_{\mu\nu} q^\nu (1 + \gamma_5)/q^2.$$

The coefficient functions are given by

$$A(B, F_2) = \sum_{q=u,c,t} U_q A_q(B_q, F_2^q), \quad (2)$$

in which $U_q = V_{qs}^* V_{qb}$ is the product of the relevant elements of the CKM matrix. As long as the u quark is ignored, one has $U_c + U_t = 0$ from unitarity of the CKM matrix. The heavy particles with masses much larger than the physical scale $\mu \approx m_b$ are integrated out and their masses are absorbed into coefficient functions evaluated in two steps [10–13]; first one computes these functions at a renormalization point about the heavy mass and then scales them down to the order of the b quark mass using the renormalization group equation. In the standard model the coefficients A_t and B_t at the scale equal to the W boson mass, for example, take the forms (with $x = m_t^2/M_W^2$)

$$\begin{aligned} A_t(x, 1) - B_t(x, 1) &= \frac{1}{4} \left[x + 3 \frac{x}{1-x} + 3 \frac{x^2}{(1-x)^2} \ln x \right], \\ B_t(x, 1) &= - \left[\frac{1}{2}x + \frac{3}{4} \frac{x}{1-x} + \frac{3}{4} \frac{2x^2 - x}{(1-x)^2} \ln x - \frac{4}{9}(\ln x + 1) \right. \\ &\quad \left. + \frac{1}{36} \frac{82x^3 - 151x^2 + 63x}{(1-x)^3} + \frac{1}{36} \frac{10x^4 + 59x^3 - 138x^2 + 63x}{(1-x)^4} \ln x \right] s_W^2. \end{aligned} \quad (3)$$

When the scale goes down, we notice first of all that as the four-fermion operator with the axial vector current of leptons has a vanishing anomalous dimension and does not mix with

other operators because of chirality, the combination $A - B$ retains its value at the higher mass scale and thus is independent of the choice of the lower scale μ . Secondly, at the level of the next-to-leading logarithm, we have

$$B_t(x, \eta) = B_t(x, 1) + B_{\text{QCD}}(\eta), \quad (4)$$

in which [14]

$$B_{\text{QCD}}(\eta) = -s_W^2 \sum_{i=1}^6 \left[\left(\frac{\pi}{\alpha_s(M_W)} p_i + s_i \right) (1 - \eta^{-a_i-1}) + r_i (1 - \eta^{-a_i}) \right]$$

enters through the mixture of the current-current and the QCD penguin four-quark operators. Here the scale-dependent parameter $\eta = \frac{\alpha_s(\mu)}{\alpha_s(M_W)}$. Finally, the magnetic-moment operator has nonzero anomalous dimension and mixes with other operators; the coefficient for it is given by [12]

$$F_2^t(x, \eta) = \eta^{-16/23} \left[\frac{1}{12} \frac{8x^3 + 5x^2 - 7x}{(1-x)^3} + \frac{1}{2} \frac{3x^3 - 2x^2}{(1-x)^4} \ln x \right. \\ \left. + (\eta^{2/23} - 1) \left(\frac{1}{3} \frac{x^3 + 5x^2 - 2x}{(1-x)^3} - \frac{2x^2}{(1-x)^4} \ln x \right) \right] \\ + 2 \sum_{i=1}^8 h_i \eta^{-a_i}. \quad (5)$$

With $\eta = 1.75$ and $m_t = 180$ GeV obtained by averaging the data of CDF and D0 groups [15], we have the values of the coefficient functions as follows

$$A_t = 2.09, \quad B_t = -0.126, \quad s_W^2 F_2^t = -0.153. \quad (6)$$

Recent measurements of $B \rightarrow X_s \gamma$ by the CLEO group [1] result in a constraint on the magnitude of F_2^t , which is close to the value of the standard model. Likewise, the dilepton decay $B \rightarrow X_s l^+ l^-$ provides a unique test of the coefficients A and B which are absent in the radiative process.

In addition to the top quark, the decay $B \rightarrow X_s l^+ l^-$ involves the charm quark and as well known, its total rate is actually dominated by the $c\bar{c}$ resonances. The contribution of these resonances such as J/ψ and ψ' to the effective Hamiltonian Eq. (1) may be taken into account by the usual form of vector-meson dominance [16–18]

$$H_V = \frac{G_F}{\sqrt{2}} U_c Q_c \left(\frac{ef_V}{M_V} \right)^2 \frac{a_2}{q^2 - M_V^2 + iM_V \Gamma_V} \bar{s} \gamma_\mu (1 - \gamma_5) b \bar{l} \gamma^\mu l,$$

where M_V is the mass of the vector intermediate state and Γ_V its full width. The decay constant is defined such that $f_V \epsilon_\mu = \langle 0 | \bar{c} \gamma_\mu c | V(\epsilon) \rangle$ and will be determined by the measured partial width for decays to lepton pairs [19]

$$\Gamma(V \rightarrow l^+ l^-) = \frac{4\pi}{3} \frac{(Q_c \alpha)^2}{M_V^3} f_V^2,$$

with $Q_c = 2/3$. In this work we treat the coupling for the neutral $b\bar{s}c\bar{c}$ four-quark operator $a_2 = c_1 + c_2/3$ as a phenomenological parameter and use the CLEO data $|a_2| = 0.26 \pm 0.03$ [20], which is close to the value determined from a fit to the rate for the semi-inclusive process $B \rightarrow X_s J/\psi$ [21]. The choice of a negative a_2 is in consistence with Breit-Wigner phase $\varphi = 0$ [22]. However, consequences of assuming a different phase for a_2 can be derived without any difficulty in principle. Hence we can read off the vector resonance component for Eq. (2),

$$A_V = B_V = \frac{16\pi^2}{3} \left(\frac{f_V}{M_V} \right)^2 \frac{a_2 s_W^2}{q^2 - M_V^2 + iM_V \Gamma_V}. \quad (7)$$

Moreover, there is an effect arising from quarks active at the μ scale, which contribute via penguin diagrams with insertion of four-quark operators. It is represented by

$$A_f = B_f = s_W^2 \left[(a_2 + a_4 + a_6) \phi(m_c^2/m_b^2, q^2/m_b^2) - \frac{a_3 + a_4 + a_6}{2} \phi(1, q^2/m_b^2) - \frac{a_3}{2} \phi(0, q^2/m_b^2) + \frac{2}{3}(a_4 + a_6) \right], \quad (8)$$

where $a_3 = c_3/3 + c_4$, $a_4 = c_3 + c_4/3$, $a_6 = c_5 + c_6/3$, and the function ϕ comes from the one-loop matrix elements of the four-quark operators and is given by

$$\phi(r_q, s) = \begin{cases} \frac{4}{3} \ln r_q - \frac{8}{9} - \frac{4}{3} \frac{4r_q}{s} + \frac{2}{3} \sqrt{1 - \frac{4r_q}{s}} \left(2 + \frac{4r_q}{s} \right) \left(\ln \frac{1 + \sqrt{1 - 4r_q/s}}{1 - \sqrt{1 - 4r_q/s}} - i\pi \right) & \left(\frac{4r_q}{s} < 1 \right); \\ \frac{4}{3} \ln r_q - \frac{8}{9} - \frac{4}{3} \frac{4r_q}{s} + \frac{4}{3} \sqrt{\frac{4r_q}{s} - 1} \left(2 + \frac{4r_q}{s} \right) \arctan \frac{1}{\sqrt{4r_q/s - 1}} & \left(\frac{4r_q}{s} > 1 \right). \end{cases}$$

Numerically, we have $a_3 = 0.0211$, $a_4 = -0.0024$, and $a_6 = 0.0028$ for $\eta = 1.75$. Comparing them with a_2 shows that the charm quark practically dominates the effect of these active quarks. Since the coupling of them to $l^+ l^-$ is of vector-type, the combination $A - B$ remains

unchanged after they are included. We remind the reader that the short-distance coefficients listed above are expressions in the NDR scheme. The scheme independence of the sum of these coefficients has been explicitly demonstrated by the authors of Ref. [12].

III. FORWARD-BACKWARD ASYMMETRY IN DILEPTON B DECAYS

A. $B \rightarrow X_s l^+ l^-$

The differential forward-backward asymmetry of the l^+ production that we are to compute is defined by

$$d\Gamma_{\text{FB}}(q^2) = \int_0^1 d\Gamma(\cos\theta_l) - \int_{-1}^0 d\Gamma(\cos\theta_l),$$

in which $\pi - \theta_l$ is the polar angle of the l^+ with respect to the direction of motion of the decaying meson in the $l^+ l^-$ frame. For the inclusive process $B \rightarrow X_s l^+ l^-$ induced by the Hamiltonian in Eq. (1), it takes the form

$$\frac{d\Gamma_{\text{FB}}}{dq^2} = \frac{1}{4\pi^3} \left(\frac{G_F}{\sqrt{2}} \right)^2 \left(\frac{\alpha}{4\pi s_W^2} \right)^2 \frac{\lambda^2 q^2}{m_b} \left(\left| B + \frac{m_b^2}{q^2} s_W^2 F_2 \right|^2 - \left| A + \frac{m_b^2}{q^2} s_W^2 F_2 \right|^2 \right), \quad (9)$$

where $\lambda = \frac{1}{2m_b} \sqrt{(m_b^2 + m_s^2 - q^2)^2 - 4m_b^2 m_s^2}$, with m_b and m_s the masses of the b and s quarks respectively. The contribution of pure photonic penguin diagrams, $\left| \frac{m_b^2}{q^2} s_W^2 F_2 \right|^2$, which governs the rate of radiative processes $B \rightarrow X_s \gamma$, cancels out. Thus the measurement of the asymmetry provides entirely independent tests of the standard model. In Eq. (9) we have set the limit of $m_l = 0$ because there is no singularity at $q^2 = 0$; so there is no mixture between left- and right-handed leptons and the difference between electron and muon channels is negligible. As noticed by the authors of Ref. [23], the forward-backward charge asymmetry is proportional to the coefficient combination $(A - B)$ and may be large for the very heavy top quark. Recalling that $(A - B)$ receives neither the QCD renormalization nor the $c\bar{c}$ effect, we anticipate that the asymmetry will become an effective measure for testing the high energy scale physics. To study its properties in detail, let us present a factorized form for the asymmetry (*integrated* over the interval of $[0, q^2]$)

$$\Gamma_{\text{FB}}(q^2) = (A - B) \left(\frac{\alpha}{4\pi s_W^2} \right)^2 \left(I_t(q^2) + s_W^2 I_f(q^2) + a_2 s_W^2 \sum_V I_V(q^2) \right). \quad (10)$$

Here I_t stands for the contributions of loops containing the virtual top quark along with QCD corrections, for which we find

$$I_t(q^2) = \frac{m_b^5 |U_t|^2}{16\pi^3} \left(\frac{G_F}{\sqrt{2}} \right)^2 \left\{ [A_t(x, \eta) + B_t(x, \eta)] \left[-\frac{1}{2}(1 - r_s)^2 s^2 + \frac{2}{3}(1 + r_s)s^3 - \frac{1}{4}s^4 \right] - 2s_W^2 F_2^t(x, \eta) \left[(1 - r_s)^2 s - (1 + r_s)s^2 + \frac{1}{3}s^3 \right] \right\}, \quad (11)$$

with $s = q^2/m_b^2$ and $r_s = m_s^2/m_b^2$. In Fig. 1 we plot the integrated asymmetries arising from the photonic penguin and the Z penguin plus W box diagrams. They are rescaled in terms of the inclusive semileptonic decay width of the B meson

$$\Gamma_{\text{s.l.}} = \frac{m_b^5 |V_{cb}|^2}{96\pi^3} \left(\frac{G_F}{\sqrt{2}} \right)^2 \tilde{f}_{bc},$$

with \tilde{f}_{bc} numerically equal to 0.39, in which we have included the one-loop QCD correction to the semileptonic B decay (all plots in this paper are rescaled in this way). For low s , photonic penguin diagrams dominate $I_t(q^2)$, and an opposite sign of F_2^t to $A_t - B_t$ in the standard model implies a positive asymmetry. As s increases, contributions of the Z penguin and W box diagrams emerge and cancel with that of photonic penguin diagrams. Consequently, the integrated asymmetry arising purely from virtual top quarks turns out to be zero at

$$s_0 = 1 - y_0 - \frac{1 - 4s_t}{9} \left[1 + \frac{1}{y_0} \left(1 - \frac{1 - 4s_t}{9} \right) \right] + \mathcal{O}\left(\frac{m_s^2}{m_b^2}\right),$$

with

$$y_0 = \frac{1}{3} \left[\frac{9}{2}(1 - 4s_t) + \frac{1}{2}(1 - 4s_t)^2 + \frac{1}{27}(1 - 4s_t)^3 + 2(1 - 4s_t)\sqrt{(2 - s_t)^2 + 2} \right]^{1/3},$$

and $s_t = -\frac{2s_W^2 F_2^t}{A_t + B_t}$. For $m_t = 180 \pm 12$ GeV and $\eta = 1.75$ we have $s_0 = 0.365 \mp 0.010$ which, by chance, is slightly below the J/ψ peak point (≈ 0.400). The range of this zero point due to the error bar of the m_t is expected to be small, considering that $(A_t + B_t)$ and F_2^t both depend rather weakly on the top mass. We find that this zero point varies

from 0.356 ∓ 0.008 to 0.381 ∓ 0.012 for the above top quark masses when η ranges from 1.50 to 2.00, which incorporates uncertainties due to QCD scale parameter as well as the renormalization subtraction point. For the top component of the short-distance coefficient, the difference between NDR and HV schemes amounts to just about 5% [13]. Thus we will see a slightly different value of the s_0 in the HV scheme. Toward the high s region the Z penguin along with W box diagram takes over in magnitude and we are left with a *surplus* of the number of l^- scattered in the *forward* hemisphere in the l^+l^- rest frame.

Other components of the pure short-distance effect, coming from active quarks, are represented by

$$I_f(q^2) = \frac{m_b^5 |U_t|^2}{6\pi^3} \left(\frac{G_F}{\sqrt{2}} \right)^2 \left\{ (a_2 + a_4 + a_6) \Phi(m_c^2/m_b^2, s) - \frac{a_3 + a_4 + a_6}{2} \Phi(1, s) - \frac{a_3}{2} \Phi(0, s) + \frac{a_4 + a_6}{2} \left[\frac{1}{2}(1 - r_s)^2 s^2 - \frac{2}{3}(1 + r_s)s^3 + \frac{1}{4}s^4 \right] \right\}, \quad (12)$$

with

$$\begin{aligned} \Phi(r_q, s) = & \left(\ln r_q - \frac{2}{3} \right) \left[\frac{1}{2}(1 - r_s)^2 s^2 - \frac{2}{3}(1 + r_s)s^3 + \frac{1}{4}s^4 \right] \\ & - 4r_q \left[(1 - r_s)^2 s - (1 + r_s)s^2 + \frac{1}{3}s^3 \right] \\ & + 16r_q^2 \left[32r_q^2 I_5(z) - 16r_q(1 + r_s + r_q)I_4(z) \right. \\ & \quad \left. + 2((1 - r_s)^2 + 4r_q(1 + r_s) - 8r_q^2)I_3(z) \right. \\ & \quad \left. - ((1 - r_s)^2 - 8r_q(1 + r_s))I_2(z) - (1 - r_s)^2 I_1(z) \right], \end{aligned} \quad (13)$$

where the explicit form for $I_k(z)$ is given in the Appendix and $z = \sqrt{1 - \frac{4r_q}{s}}$. Figure 2 summarizes asymmetries coming from the short-distance effects alone. The nonresonant $c\bar{c}$ component dominating active quark effects becomes substantial above the threshold $2m_c$. Unfortunately, the total short-distance contribution suffers from a cancellation between the top and $c\bar{c}$ components, which reduces strongly the surplus of l^- of high q^2 in the forward hemisphere. With the same reasoning, we expect a vanishing net result of the short-distance effect as a whole somewhere in the middle region of the phase space. This sort of zero points (denoted by \bar{s}_0) is identical in the NDR and HV schemes. To be precise, we evaluate the

position of this point for $m_t = 180 \pm 12$ GeV and $\eta = 1.75$. It turns out to be $\bar{s}_0 = 0.511 \mp 0.025$, which comes closer to the ψ' resonance than the J/ψ . We find a weak η dependence of this zero point and obtain a derivation less than 4% for η varying from 1.50 to 2.00 once again.

Now let us consider resonant effects arising from vector intermediate states. We have

$$I_V(q^2) = \frac{2m_b f_V^2 |U_t|^2}{3\pi r_V} \left(\frac{G_F}{\sqrt{2}} \right)^2 \left[[(1+r_s-r_V)^2 - 4r_s]s - \frac{1}{2}[2(1+r_s) - r_V]s^2 + \frac{1}{3}s^3 \right. \\ \left. + r_V [(1-r_V)^2 + 2(1+r_V)r_s - r_s^2] \ln \sqrt{(1 - \frac{s}{r_V})^2 + \sigma_V^2} \right. \\ \left. + \mathcal{O}(\sigma_V) \right], \quad (14)$$

with $r_V = M_V^2/m_b^2$ and $\sigma_V = \Gamma_V/M_V$. The resonant component $I_V(q^2)$ reaches its maximum value at $s = r_V$. Because of the dependence on the real part of the resonant propagator, as s passes through r_V , the differential asymmetry changes sign. There is, therefore, a partial cancellation of the $I_V(q^2)$ and instead of a plateau we will find a decreasing integrated asymmetry for s across the mass of the vector resonance.

The integrated asymmetry of the l^+ production in the inclusive process $B \rightarrow X_s l^+ l^-$ is plotted in Fig. 3 and includes the components of J/ψ and ψ' resonances. It is characterized by prominent peaks at $q^2 = M_{J/\psi}^2$ and $M_{\psi'}^2$, respectively in the resonant region, as expected. The contribution of the ψ' resonance is around one third that of the J/ψ . In the J/ψ resonant region, the top quark component of the asymmetry is actually small, as explained previously. It means that the product $a_2(A - B)$ dominates, as far as the coefficients are concerned. Unlike the decay rate, the $(A - B)$ is involved here linearly. Alternatively stated, the short-distance effects as a whole disappears at \bar{s}_0 , which is near the ψ' . The asymmetry, therefore, appears in the shape of the real part of the resonant propagator. Experimentally, a_2 has been reasonably well extracted from the CLEO data and hopefully more precise data will come from the planned B factories. As a result, the prediction for asymmetries near these zero points (or resonances) can be made in a way insensitive to the QCD renormalization parameter η . Numerically, as η ranges from 1.50 to 2.00, $\Gamma_{\text{FB}}(M_{J/\psi}^2)$, for example, varies

merely by 6.1%. In our opinion, measurements of these asymmetries will be an effective way to unambiguously test the combination $A - B$ arising purely from short-distance physics. Meanwhile, as $A - B$ depends strongly on the top mass in the standard model, it may be an independent way to confirm the value of m_t determined in different ways.

B. $B \rightarrow K^* l^+ l^-$

We now turn our attention to the exclusive channel $B \rightarrow K^* l^+ l^-$. The effective quark current $\bar{s}\Gamma_\mu^{A(B)}b$ in question has two different structures; the parametrization for the matrix element of $V - A$ currents in terms of invariant form factors is

$$\begin{aligned} \langle p, \phi | \bar{s}\gamma^\mu(1 - \gamma_5)b | P \rangle &= [a_+(q^2)(P + p)_\mu + a_-(q^2)(P - p)_\mu]P^\nu\phi_\nu^* \\ &+ f(q^2)\phi_\mu^* + ig(q^2)\epsilon_{\mu\nu\alpha\beta}\phi^{*\nu}P^\alpha p^\beta. \end{aligned} \quad (15)$$

In analogy to this we have for the magnetic-moment operator

$$\begin{aligned} -\frac{i}{q^2}\langle p, \phi | \bar{s}\sigma_{\mu\nu}q^\nu(1 + \gamma_5)b | P \rangle &= [\tilde{a}_+(q^2)(P + p)_\mu + \tilde{a}_-(q^2)(P - p)_\mu]P^\nu\phi_\nu^* \\ &+ \tilde{f}(q^2)\phi_\mu^* + i\tilde{g}(q^2)\epsilon_{\mu\nu\alpha\beta}\phi^{*\nu}P^\alpha p^\beta, \end{aligned} \quad (16)$$

along with a condition of current conservation,

$$(M^2 - m^2)\tilde{a}_+ + q^2\tilde{a}_- + \tilde{f} = 0.$$

Here M (P_μ) and m (p_μ) are masses (momenta) of B and K^* mesons, respectively, ϕ_μ the polarization vector of the K^* meson (satisfying $\phi_\mu p^\mu = 0$) and $q = P - p$ the momentum transfer into the dilepton.

The differential forward-backward asymmetry of $B \rightarrow K^* l^+ l^-$ reads [6]

$$\frac{d\Gamma_{\text{FB}}}{dq^2} = \frac{1}{64\pi^3} \left(\frac{G_F}{\sqrt{2}}\right)^2 \left(\frac{\alpha}{4\pi s_W^2}\right)^2 \frac{\lambda q^2}{M^2} [(|H_+^L|^2 - |H_-^L|^2) - (|H_+^R|^2 - |H_-^R|^2)], \quad (17)$$

where necessarily now $\lambda = \frac{1}{2M}\sqrt{(M^2 + m^2 - q^2)^2 - 4M^2m^2}$. The helicity amplitudes appearing here are defined as

$$H_\pm^{L(R)} = A(B)h_\pm + m_b s_W^2 F_2^t \tilde{h}_\pm, \quad (18)$$

where $h_{\pm} \equiv f \pm \lambda M g$ [24] and $\tilde{h}_{\pm} \equiv \tilde{f} \pm \lambda M \tilde{g}$. Assuming the B meson contains an on-shell b quark of velocity v , one finds

$$\tilde{h}_{\pm} = \frac{1}{q^2} (M - v \cdot p \mp \lambda) h_{\pm}. \quad (19)$$

(see Ref. [5,6] for detailed discussion.) With these relations we may rewrite the differential asymmetry of Eq. (16) as

$$\begin{aligned} \frac{d\Gamma_{\text{FB}}}{dq^2} &= \frac{1}{64\pi^3} \left(\frac{G_F}{\sqrt{2}} \right)^2 \left(\frac{\alpha}{4\pi s_W^2} \right)^2 \frac{\lambda q^2}{M^2} (A - B) \\ &\times \left[|h_+|^2 \left(A + B^* + 2s_W^2 F_2 \frac{M - v \cdot p - \lambda}{q^2/m_b} \right) - |h_-|^2 \left(A + B^* + 2s_W^2 F_2 \frac{M - v \cdot p + \lambda}{q^2/m_b} \right) \right]. \end{aligned} \quad (20)$$

Certainly, further analysis requires the knowledge of hadronic form factors, but it is hard to calculate them directly from the first principles of QCD. In Ref. [5,6] we have used heavy flavor symmetry to relate the form factors for $B \rightarrow K^* l^+ l^-$ decays with those for $D \rightarrow K^* l^+ \nu$. In the leading order of heavy quark effective theory, form factors scale as [25]

$$\begin{aligned} f &= \left[\frac{\alpha_s(m_b)}{\alpha_s(m_c)} \right]^{-6/25} \sqrt{\frac{M}{M_D}} f_D, \\ g &= \left[\frac{\alpha_s(m_b)}{\alpha_s(m_c)} \right]^{-6/25} \sqrt{\frac{M_D}{M}} g_D. \end{aligned} \quad (21)$$

In this equation form factors are evaluated at the same $v \cdot p$, namely that f and g at $q^2 = M^2 + m^2 - 2Mv \cdot p$ are related to f_D and g_D at $q_D^2 = M_D^2 + m^2 - 2M_D v \cdot p$. Thus the whole physical range of $q_D^2 = [0, (M_D - m)^2]$ in $D \rightarrow K^*$ covers $q^2 = [q_0^2, (M - m)^2]$ in $B \rightarrow K^*$, where $q_0^2 = (4.07 \text{ GeV})^2$. With the data available for $D \rightarrow K^*$ we are led to a reliable estimate of the asymmetry in the region above the ψ' resonance, on the basis of momentum-to-momentum correspondence of form factors [6]. However, extrapolating the data of D decays to lower q definitely needs the knowledge of the q^2 -dependence for form factors. In this work we will employ the pole dominance approximation,

$$\left(1 - \frac{q^2}{M^2} \right)^n h(q^2) = \left(1 - \frac{q_0^2}{M^2} \right)^n h(q_0^2); \quad (h = f, g). \quad (22)$$

Here M' is the pole mass of the current involving b and s quarks and we make no distinction between the vector and axial vector masses. While this form seems reasonable for the small recoil region of $B \rightarrow K^*$ decays, as the end-point is close to the pole, we hope it helps to figure out the properties of forward-backward asymmetries in the resonant region or below. Regarding poles of degree n , we make use of two schemes; one assumes the monopole form for both f and g like the BSW model [26], and another follows the suggestion of Körner and Schuler [27], namely $n = 1$ for f , but a dipole form of $n = 2$ for g (The latter is referred to as the dipole scheme in this paper despite f actually being of monopole form.). Meanwhile, Eq. (20) will be used to obtain form factors at the kinematical point q_0 ; so with form factors $A_1(0)$ and $V(0)$ (they are linear combinations of f_D and g_D) of $D \rightarrow K^*(892) l^+ \nu$ measured by E691, E687 and CLEO groups [28], one ends up with $f_D(0) = -1.43$ GeV and $g_D(0) = 0.695$ GeV $^{-1}$, which translate to $f(q_0^2) = -2.64$ GeV and $g(q_0^2) = 0.455$ GeV $^{-1}$.

Before doing practical calculations, we perform a simple analysis of integral asymmetries, by using the monopole form factor along with the limit of $M = M'$ and $m^2/M^2 \ll 1$. It ought to be appropriate for the region not close to the pole, say around the J/ψ mass or below. In this case, the counterpart of Eq. (11) in the K^* mode, with necessarily $s = q^2/M^2$ for this moment, has the form

$$I_t^{(K^*)}(q^2) = \frac{M^5 |U_t|^2}{128\pi^3} \left(\frac{G_F}{\sqrt{2}} \right)^2 \left\{ f_0 g_0 [A_t(x, \eta) + B_t(x, \eta)] s^2 - 2s_W^2 F_2^t(x, \eta) \left[\left(\frac{f_0}{M} - \frac{Mg_0}{2} \right)^2 s - \frac{Mg_0}{2} \left(\frac{f_0}{M} + \frac{Mg_0}{2} \right) s^2 + \frac{1}{3} \left(\frac{Mg_0}{2} \right)^2 s^3 \right] \right\}. \quad (23)$$

We have defined that $f_0 = f(0)$ and $g_0 = g(0)$. Once again, competition between photon penguin and Z penguin plus W box diagrams causes a zero point of $I_t^{(K^*)}$ at

$$\frac{3}{2} \left(1 - 2 \frac{(2-s_t)}{s_t} \frac{f_0}{M^2 g_0} \right) \left[1 - \sqrt{1 - \frac{4}{3} \left(\frac{1 - 2 \frac{f_0}{M^2 g_0}}{1 - 2 \frac{(2-s_t)}{s_t} \frac{f_0}{M^2 g_0}} \right)^2} \right]. \quad (24)$$

Clearly, as $s_t < 1$ in the standard model, the condition that f_0 is of opposite sign to g_0 guarantees a real value of this root. This condition is satisfied physically because the helicity

relation $|h_+| < |h_-|$ has been well confirmed in semileptonic decays [24], namely that the $V - A$ structure of the quark current is manifested at the hadron level. Numerically, with $f(q_0^2)$ and $g(q_0^2)$ given earlier the zero point turns out to be 0.345 ∓ 0.07 for $m_t = 180 \pm 12$ GeV and $\eta = 1.75$. It coincides with the J/ψ peak $M_{J/\psi}^2/M^2 = 0.344$.

Meanwhile, the correspondence to Eq. (12) reads

$$I_f^{(K^*)}(q^2) = \frac{M^5 |U_t|^2}{24\pi^3} \left(\frac{G_F}{\sqrt{2}} \right)^2 f_0 g_0 \left[(a_2 + a_4 + a_6) \Phi^{(K^*)}(m_c^2/M^2, s) - \frac{a_3}{2} \Phi^{(K^*)}(0, s) - \frac{a_3 + a_4 + a_6}{2} \Phi^{(K^*)}(1, s) - \frac{a_4 + a_6}{4} s^2 \right], \quad (25)$$

with

$$\Phi^{(K^*)}(r_q, s) = 4r_q s - \frac{1}{2}(\ln r_q - \frac{2}{3})s^2 - 16r_q^2[2I_3(z) - I_2(z) - I_1(z)]. \quad (26)$$

In analogy to the inclusive process, adding the active quark effect to the top one ends up with a cancellation of the asymmetry once again. We find a complete cancellation at $\bar{s}_0 = 0.451 \mp 0.012$ for the same top mass and η as before. In addition we work out the vector resonant contribution which is

$$I_V^{(K^*)}(q^2) = -\frac{M f_V^2 |U_t|^2}{6\pi} \left(\frac{G_F}{\sqrt{2}} \right)^2 f_0 g_0 \left(\frac{s}{r_V} + \ln \sqrt{\left(1 - \frac{s}{r_V}\right)^2 + \sigma_V^2} + \mathcal{O}(\sigma_V) \right), \quad (27)$$

where now $r_V = M_V^2/M^2$. We should remark that the above expressions illustrate the features of the asymmetries in $B \rightarrow K^* l^+ l^-$, viz., the peaks in the resonant contribution, the cancellation between Z penguin and plus W box diagrams, and the plateau in the nonresonant $c\bar{c}$ effect above the threshold $2m_c$. In particular, we found the position of the zero point for the short-distance effect is in good agreement with what we obtained via the full expression.

Nevertheless, if we still ignored the K^* mass in the region near the endpoint, the phase space would approach $q^2 = M^2$ rather than $(M - m)^2$. While it may make a slight difference in the inclusive process (where m is replaced by m_s), this small change in the upper boundary of phase space could lead to a sizeable overestimate of observable quantities such as the decay rate and asymmetry in exclusive channels. This is because the pole in the form factors

dominates the distribution at the endpoint. The shift of the pole mass to M would further increase the estimate. Thus when the whole range of q^2 in the decay $B \rightarrow K^*$ is considered, we apply the full expression of Eq. (19) (using the experimental values for the masses m and M'). In this way, the integrated asymmetry for $B \rightarrow K^*l^+l^-$ is plotted in Fig. 4 for monopole and dipole form factors. We have checked that there is a variation of the zero point of short-distance effects due to the choice of form factors. With the same m_t and η as before, there are $s_0 = 0.338 \mp 0.007$ (the top quark effect alone) and $\bar{s}_0 = 0.511 \mp 0.017$ (the short-distance effect as a whole) for the monopole scheme, as well as 0.291 ∓ 0.006 and 0.444 ∓ 0.013 for the dipole one. The contribution of J/ψ along with the $c\bar{c}$ effect still dominates its resonant region. By comparison, we find the two schemes of form factors give similar results of the integrated asymmetry above the ψ' . This is expected when both schemes use the data of semileptonic D decays as input. But asymmetries, integrated over the interval between the J/ψ and ψ' and the region below the J/ψ with the monopole form, are 1.7 times as large as that with the dipole one. This factor becomes even larger when q^2 is near to the origin. For the monopole form, a fraction of 25% or so of the asymmetry occurs in the ground state and this is far from saturating the inclusive process. So it is anticipated that higher K -resonances may play an important role in measuring asymmetry as well.

IV. DISCUSSION AND CONCLUSION

As we have seen in Fig. 1, the magnetic-moment operator becomes important for photons approaching the mass-shell. The positive asymmetry arising from it is the consequence of the coefficient F_2^t being negative relative to $A - B$ in the standard model. Thus measurement in this region will tell us the sign of F_2^t , as well as confirming its bound given by the decay $b \rightarrow s\gamma$.

On the other hand, the relative phase between F_2^t and $A_t + B_t$ impacts dramatically on the $b \rightarrow sl^+l^-$. For example, a potential magnetic-moment operator of a similar size but opposite sign to that in the standard model, such as those allowed in supersymmetry models

[29], may increase the forward-backward asymmetry of the whole kinematical region by a factor of $4.0 \sim 5.0$ and a factor 2.0 for that in the low q region with a cut-off at $M_{J/\psi}$, but reversing the sign of the asymmetry. In fact, if this relative phase is negative it shows us evidence of new physics, whereas if it is positive it leads to the sensitivity of the asymmetry with respect to the J/ψ and the $c\bar{c}$ continuum in the middle region. We emphasize that the relative phase between F_2^t and $A_t + B_t$ manifests itself as well in the invariant mass spectrum of dileptons. When left-handed leptons do not mix up with right-handed ones in the massless lepton limit, the only interference occurs between quarks outgoing from the four-fermion vertex and that from the penguin, yielding a term proportional to $\text{Re}[(A_t + B_t)F_2^t]$ in the dilepton spectrum. As it is likely that the first experiment will be carried out for this spectrum, we will be able to see whether there is cancellation between the top quark components of the asymmetry in a model independent way.

Toward high q^2 , coefficients A_t and B_t become important as they are enhanced by an extra q^2 . The contributions of Z boson penguin along with W box diagrams in this region surpass that of the photonic penguin diagram for a large top quark mass such as 174 GeV (see Eq. (6)). While $A - B$ (and F_2^t) may be determined by the method described before, this asymmetry will help to extract the value of the combination $A_t + B_t$ experimentally. When B_t always occurs in combinations with the much larger A_t , any appreciable difference between $A_t + B_t$ and $A_t - B_t$ is beyond the standard model.

As for the exclusive decay $B \rightarrow K^*l^+l^-$, the difference between the two assumptions about form factors becomes evident for low q . When applied to the rare radiative decay $B \rightarrow K^*\gamma$, the monopole form factors give a theoretical value of 17% for the ratio of the exclusive to inclusive rate, defined as $R = \frac{\Gamma(B \rightarrow K^*\gamma)}{\Gamma(B \rightarrow X_s\gamma)}$. This is favored by the preliminary CLEO data [1], while the dipole scheme result of 5.7% is not. Although these two sets of form factors are similar to each other near the endpoint, we tend to favor the prediction for charge asymmetries obtained by using the monopole scheme, as far as the whole kinematical region is concerned.

Finally we want to point out that possible experimental cuts in the invariant mass of

lepton-antilepton pairs do not necessarily mean loss of statistics as far as asymmetry is concerned. For instance, a cut-off at the J/ψ mass from which we integrate to the endpoint q_{\max} leads to an asymmetry larger in magnitude than that over the whole kinematical region. In fact, this interval gives the maximum integrated asymmetry because of the resonant enhancement. Our prediction for it, using $m_t = 180$ GeV, is $-1.54 \times 10^{-5} \Gamma_{s.l.}$ in the inclusive process, which is accessible in the upcoming B factories.

In conclusion we have presented a comprehensive analysis of forward-backward asymmetry of l^+ production in the decay $B \rightarrow X_s l^+ l^-$ and $B \rightarrow K^* l^+ l^-$. We have attempted to specify certain regions in phase space of the B decay in which the asymmetry is sensitive to individual short-distance coefficients. In particular, we note the potential importance of the J/ψ , since the integrated asymmetry near its resonant region is largely independent of the QCD renormalization. Given the strong dependence of $A - B$ on the top quark mass, measurements of this asymmetry will not only provide an effective test of the standard model but also lead to information about m_t . As well, we believe that the shape of the plots in Figs. 1 to 4 represent well the expectation for the forward-backward asymmetry in the framework of the standard model. Therefore if future experiments observe any dramatic deviation from them, they can be regarded as the evidence of new physics beyond the standard model.

ACKNOWLEDGMENTS

The author thanks R. Delbourgo for many discussions and encouragement along with N. Jones for his help in preparation of this letter. He is also grateful to the Australian Research Council for their financial support, under grant number A69231484.

APPENDIX: INTEGRAL FORMULAE

When the effect of the one-loop matrix element is studied in the main text, we have used the notation $I_k(z)$ for the integral defined as

$$I_k(z) = \text{Re} \left[\int_{z_0}^z \frac{du}{(1-u^2)^k} \left(\ln \frac{1+u}{1-u} - i\pi \right) \right] \quad (k = 1, 2, \dots).$$

It holds in both ranges above and below the threshold $2m_q$. In the latter case where u is imaginary, we apply the analytic continuation

$$\arctan \left(\frac{1}{|u|} \right) = \frac{i}{2} \left(\ln \frac{1+u}{1-u} - i\pi \right).$$

The lower limit z_0 corresponds to $q^2 = 0$. It is not difficult to work out I_k for $k = 1$

$$I_1(z) = \frac{1}{2} \text{Re} \left[\ln \frac{1+u}{1-u} \left(\frac{1}{2} \ln \frac{1+u}{1-u} - i\pi \right) \right]_{z_0}^z.$$

We would like to present in this appendix a general procedure to carry out the integral for arbitrary k . To this end, it is convenient to consider an auxiliary function

$$\mathcal{I}(z; a) = \text{Re} \left[\int_{z_0}^z \frac{du}{(a-u^2)} \left(\ln \frac{1+u}{1-u} - i\pi \right) \right] \quad (a > 0),$$

and thus the integral in question may be rewritten as

$$I_k(z) = \frac{(-1)^{(k-1)}}{(k-1)!} \frac{\partial^{(k-1)} \mathcal{I}(z; a)}{\partial a^{(k-1)}} \Big|_{a=1}.$$

Hence it is straightforward to derive the $I_k(z)$ for any k larger than one with the explicit form of $\mathcal{I}(z; a)$ in terms of a series

$$\begin{aligned} \mathcal{I}(z; a) = \frac{1}{\sqrt{a}} I_1(z) - \frac{1}{2\sqrt{a}} \sum_{l=1}^{\infty} \frac{(1-\sqrt{a})^l}{l} \text{Re} \left\{ J_l^- - J_l^+ + \frac{1}{l} \left[\frac{1}{(1+u)^l} + \frac{1}{(1-u)^l} \right] \right. \\ \left. + \left[\frac{1}{(1+u)^l} - \frac{1}{(1-u)^l} \right] \left(\ln \frac{1+u}{1-u} - i\pi \right) \right\}_{z_0}^z, \end{aligned}$$

in which J_l^\pm is given by the recurrence

$$J_l^\pm = \int \frac{du}{(1 \pm u)^l} \frac{1}{(1 \mp u)} = \frac{1}{2} \left[\mp \frac{1}{(l-1)} \frac{1}{(1 \pm u)^{l-1}} + J_{l-1}^\pm \right],$$

where we know the starting values

$$J_1^+ = J_1^- = \frac{1}{2} \ln \frac{1+u}{1-u}.$$

REFERENCES

- [1] CLEO Collab., R. Ammar et al., Phys. Rev. Lett. **71**, 674 (1993); E. Thorndike, in Proc. of the American Physical Society Meeting, Washington (DC), April 1993; T. Browder, K. Honscheid and S. Playfer, CLNS 93/1261, UH-511-778-93-018, HEPSY 93-10 (1993); B. Barish et al., preprint CLEO CONF 94-1.
- [2] For example, see A. Ali, C. Greub and T. Mannel, DESY Report 93-016(1993), A. Ali, ECFA report 93/151, DESY 93-053(1993) and references cited therein.
- [3] N. G. Deshpande, K. Panose and J. Trampetic, Phys. Lett. **B308**, 322 (1993).
- [4] A. Ali, G. F. Giudice, and T. Mannel, CERN-TH 7346/94.
- [5] R. Delbourgo and Dongsheng Liu, Phys. Rev. **D51**, 118(1995).
- [6] Dongsheng Liu, Phys. Lett. **B346**, 355 (1995).
- [7] C. Greub, A. Ioannissian, and D. Wyler, Phys. Lett. **B346**, 149 (1995).
- [8] A. J. Buras and M. Muenz, MPI-PhT/94-60 and TUM-T31-75/94.
- [9] N. G. Deshpande and J. Trampetic, Phys. Rev. Lett. **60**, 2583 (1988).
- [10] T. Inami and C. S. Lim, Prog. Theor. Phys. **65**, 297 (1981).
- [11] B. Grinstein, M. J. Savage and M. B. Wise, Nucl. Phys. **B319**, 271 (1989); R. Grigani, P. J. O'Donnell, M. Sutherland and H. Navelet, Phys. Lett. **B223**, 239 (1989); G. Cella, G. Ricciardi and A. Vicere, Phys. Lett. **B258**, 212 (1991).
- [12] M. Misiak, Nucl. Phys. **B393**, 23 (1993) and ERRATUM, ibid. **B439**, 461 (1995).
- [13] A. J. Buras and M. Muenz, MPI-PhT/94-96 and TUM-T31-82/94.
- [14] The anomalous dimensions a_i along with the coefficients p_i , s_i , and r_i as well as afterwards, h_i and c_i are given in refs. [12,13].

- [15] CDF Collab., F. Abe et al., FERMILAB-PUB-95/022-E; D0 Collab., S. Abachi et al., FERMILAB-PUB-95/028-E.
- [16] N. G. Deshpande, J. Trampetic and K. Panose, Phys. Rev. **D39**, 1461 (1989).
- [17] C. S. Lim, T. Morozumi and A. I. Sanda, Phys. Lett. **B218**, 343 (1989).
- [18] C. A. Deominguez, N. Paver and Riazuddin, Z. Phys. **C48**, 55 (1990).
- [19] Particle Data Group, Phys. Rev. **D50**, Part I (Aug. 1994).
- [20] CLEO Collab., M. S. Alam et al., Phys. Rev. **D50**, 43 (1994).
- [21] N. G. Deshpande and J. Trampetic, OITS-546.
- [22] P. J. O'Donnell and H. K. K. Tung, Phys. Rev. **D43**, 2067 (1991).
- [23] A. Ali, T. Mannel, and T. Morozumi, Phys. Lett. **B273**, 505 (1991).
- [24] J. G. Kröner and G. A. Schuler, Phys. Lett. B226 (1989) 185; F. J. Gilman and R. L. Singleton, Phys. Rev. D41 (1990) 142.
- [25] N. Isgur and M. B. Wise, Phys. Rev. D42 (1990) 2388.
- [26] M. Wirbel, B. Stech and M. Bauer, Z. Phys. **C29**, 637 (1985).
- [27] J. G. Körner and G. A. Schuler, Z. Phys. **C38**, (1988) 511.
- [28] E691 Collab., J. C. Anjos et al., Phys. Rev. Lett. 65 (1990) 2630; E653 Collab., K. Kodama et al., Phys. Lett. B274 (1992) 246; Phys. Lett. B286 (1992) 187. E687 Collab., P. L. Frabetti et al., Phys. Lett. B307 (1993) 262.
- [29] S. Bertolini, F. Borzumati and A. Masisero, Nucl. Phys. B353 (1991) 591.

Figure captions:

Figure 1 The top quark components of forward-backward charge asymmetry in the decay $B \rightarrow X_s l^+ l^-$, *integrated* over the region of $[0, q^2]$. The dashed line corresponds to the photon penguin diagram, while the solid to Z penguin plus W box diagrams. We take the values $m_t = 174$ GeV, $\eta = 1.75$, and $m_b = 4.9$ GeV and the limit of $m_s^2/m_b^2 \rightarrow 0$. Both plots are rescaled by the semileptonic decay width of the B meson, multiplied by the factor of 10^5 .

Figure 2 Integrated asymmetries due to short-distance effects in $B \rightarrow X_s l^+ l^-$. The dashed line corresponds to the active $q\bar{q}$ contribution dominated by the $c\bar{c}$, and the solid to the top quark one, that is the sum of plots in Fig. 1. We use $m_c = 1.5$ GeV and the remaining parameters and the scale are the same as in Fig. 1.

Figure 3 The same as in Figs. 1 and 2 for the sum (dashed line) of all effects (see Eq. (10) in the main text), including resonant contributions (solid line).

Figure 4 Integrated forward-backward asymmetries in the decay $B \rightarrow K^* l^+ l^-$. The dashed line is associated with the monopole scheme of form factors, while the solid line goes with the dipole one. We take $M = 5.28$ GeV, $m = 0.892$ GeV, and $M' = 5.38$ GeV. The remaining parameters and the scale are the same as in previous figures.

FIGURES

$$\frac{\Gamma_{\text{FB}}}{\Gamma_{\text{s.l.}}}$$

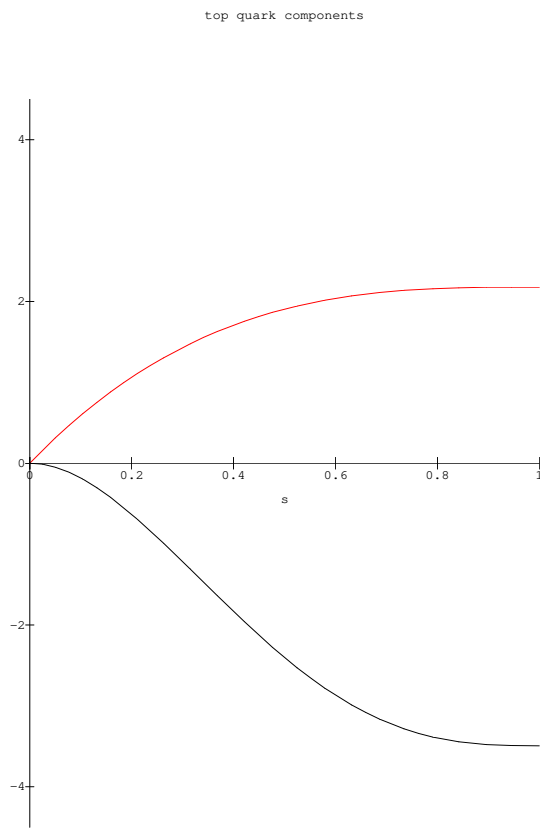


FIG. 1. D. Liu

$$\frac{\Gamma_{\text{FB}}}{\Gamma_{\text{s.l.}}}$$

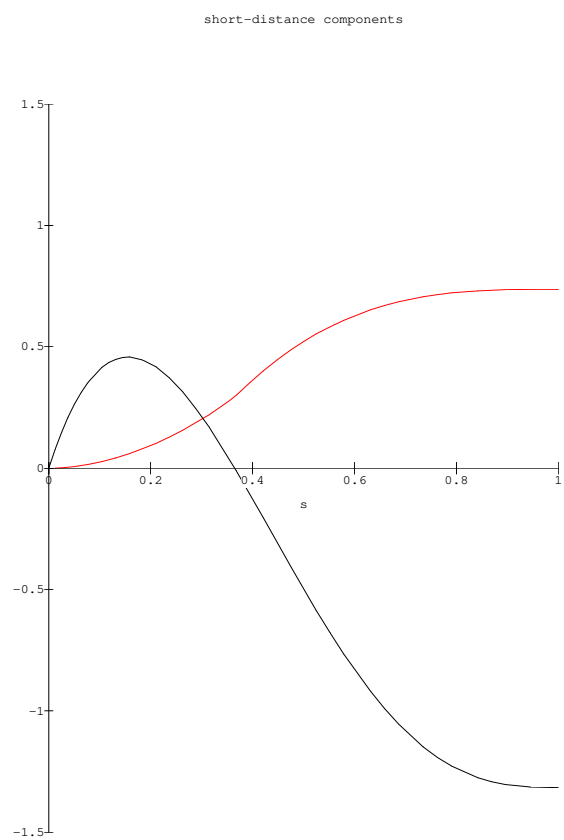


FIG. 2. D. Liu

$$\frac{\Gamma_{FB}}{\Gamma_{s.l.}}$$

Forward-backward asymmetry in $B \rightarrow Xs l \bar{l}$

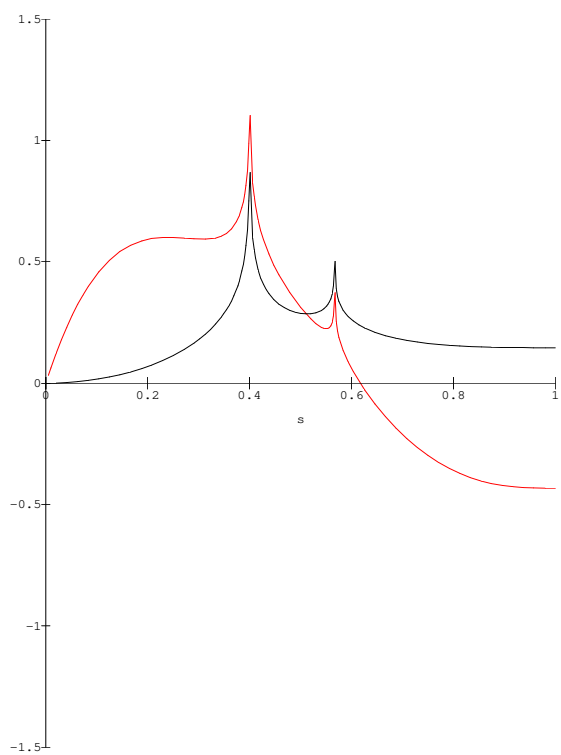


FIG. 3. D. Liu

$$\frac{\Gamma_{\text{FB}}}{\Gamma_{\text{s.l.}}}$$

Forward-backward asymmetry in $B \rightarrow K^* \ell \bar{\ell}$

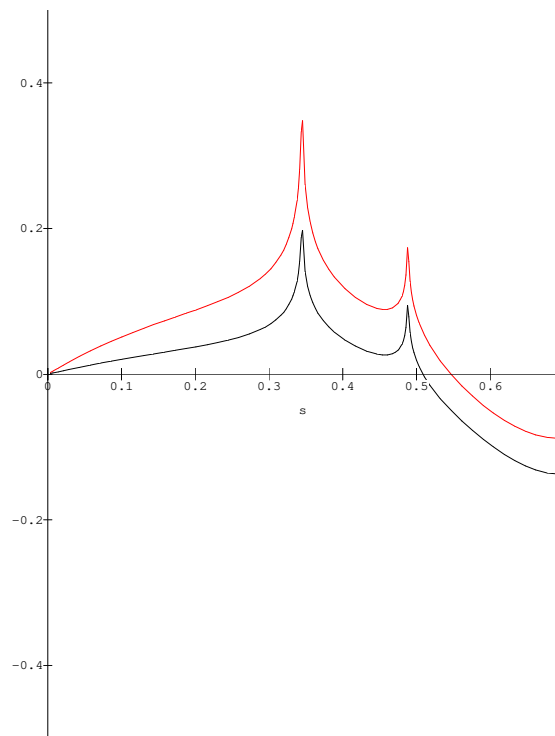


FIG. 4. D. Liu

This figure "fig1-1.png" is available in "png" format from:

<http://arxiv.org/ps/hep-ph/9505314v2>

This figure "fig1-2.png" is available in "png" format from:

<http://arxiv.org/ps/hep-ph/9505314v2>

This figure "fig1-3.png" is available in "png" format from:

<http://arxiv.org/ps/hep-ph/9505314v2>

This figure "fig1-4.png" is available in "png" format from:

<http://arxiv.org/ps/hep-ph/9505314v2>